Laser cladding of Inconel 625 wire for corrosion protection

T.E. Abioye [a], D.G. McCartney [b], A.T. Clare [a,*]

[a] Division of Manufacturing, Faculty of Engineering, University of Nottingham, Nottingham NG7 2RD, UK
[b] Division of Materials, Mechanics and Structures, Faculty of Engineering, University of Nottingham, Nottingham NG7 2RD, UK

ARTICLE INFO

ABSTRACT

The electrochemical corrosion performance of laser clad Inconel 625 wire in a de-aerated 3.5 wt% NaCl solution was investigated. The microstructure of the clad beads before and after the corrosion testing was examined using a combination of optical microscopy, scanning electron microscopy (with energy dispersive X-ray analysis) and X-ray diffraction. Well bonded, minimally diluted, pore- and crack-free single bead and multiple (overlapped) beads of Inconel 625 wire were successfully deposited. The clad beads comprise dendritic γ-Ni (FCC) matrix and interdendritic precipitates which are Mo- and Nb-rich. The microstructural evolution of a typical clad bead is observed to begin with columnar dendrites, at the clad-substrate interface, growing vertically to the substrate. This blends into horizontal columnar dendrites near the top region. High integrity laser coating (multiple beads) of Inconel 625 wire with a minimal dilution ratio of 4.5% is found in this study. The corrosion performance of the coating, which degrades with increasing Fe dilution, is very close to that of wrought Inconel 625 but superior to the wrought 304L stainless steel. The stainless steel exhibited localised (pitting) corrosion however, it was fully protected by the Inconel 625 wire laser coating in the saline solution.

1. Introduction

Surface modification of engineering components for protection against corrosion is a critical field of research in the oil and gas industry. Among the various coating techniques for surface modification of ferrous metals, laser cladding offers advantages over other conventional techniques such as thermal spraying and arc weld. Huang (2011) revealed that laser cladding has the potential to produce coatings with low substrate dilution, minimal distortion and strong metallurgical bonding with the substrate. However, Zhou et al. (2008a,b) has reported that high propensity for crack formation, which is due to rapid meltpool solidification, has been a major drawback of laser cladding processes. Cracking is detrimental to the corrosion performance of the laser coatings because they act as sites for crevice and pitting corrosion. It also offers interconnected path to the substrate. Further research by Zhou et al. (2008a,b) revealed that cracking in the laser clad layers can be avoided by optimising the processing parameters, preheating the substrate prior laser deposition and cladding with alloys of high ductility.

According to Al-fadhli et al. (2006), Inconel 625 exhibits high corrosion resistance and high ductility which make it a material of choice for surface modification of oil and gas components,

especially those made with stainless steel. Hence, the life span of industrial parts is being extended in severe corrosive media by this method. Inconel 625 is a non-magnetic nickel–chromium–molybdenum nickel-based superalloy strengthened mainly by solid solution hardening effect of the refractory metals, niobium and molybdenum in an austenitic FCC γ matrix. It is also precipitation hardenable due to the precipitation of γ'' (Ni$_3$Nb) after annealing over a long period in the temperature range 550–580 °C (Paul et al., 2007). It often finds applications where high temperature strength and excellent corrosion resistance in a wide range of corrosive media are required (Donachie and Donachie, 2002). Dinda et al. (2009) reported that chromium and nickel provide resistance in oxidising environments while molybdenum and nickel resist any form of non-oxidising corrosion. Chromium continuously passivates the external surface of the alloy by forming Cr$_2$O$_3$ which is the primary reason for resistance to corrosion. The presence of molybdenum (8–10 wt%) is good for resistance against crevice and pitting corrosion. Kim et al. (2007) investigated the weldability of the Inconel 625 alloy coatings. It was discovered that the high ductility of the alloy 625 contributes to its ability to prevent solidification cracking after welding.

Most of the previous works on Inconel 625 laser coating for corrosion protection were performed using powder as the feedstock material. Tuominen et al. (2003) studied the electrochemical performance of Inconel 625 powder coatings deposited by HVOF and laser cladding techniques in de-aerated 3.5 wt% NaCl solution. It

* Corresponding author. Tel.: +44 0 115 951 4109; fax: +44 0 115 951 3800.
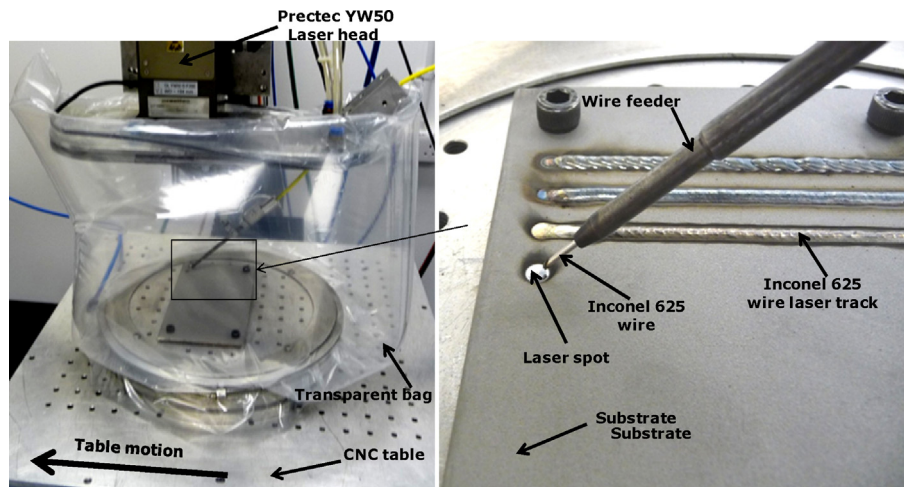E-mail address: adam.clare@nottingham.ac.uk (A.T. Clare).

Fig. 1. Experimental arrangement for Inconel 625 wire laser deposition.

was found that the laser coating demonstrated higher corrosion resistance in terms of lower passive current density, higher breakdown potential and corrosion potential. The lower performance of HVOF coating was attributed to inhomogeneous coating structure caused by pores and oxide formation alongside the presence of interconnected paths which were absent in the laser coating. Ahmed (2008) also revealed that the corrosion performance, in a saline media, of Inconel 625 powder clad layer is close to that of wrought Inconel 625 but superior to HVOF coatings. Also, the corrosion behavior of fusion cladded and explosive cladded Inconel 625 alloy has been studied by Zareie Rajani et al. (2013). It was found that high Fe content is detrimental to the corrosion properties of the alloy 625 claddings.

To date, only few articles exist on the processing and property of wire clad Inconel 625 coatings. Nurminen (2008) has researched on the hot-wire laser cladding. Also, corrosion resistant laser coatings for hydraulic piston rods using wire as the feedstock material has been a subject of investigation by Tuominen et al. (2012). Compared with powder fed methods, laser cladding with wire has the potential to give cleaner process environment, higher material deposition efficiency, improved surface quality and reduced material wastage which serve to improve process economy. The tendency for pore formation as a result of entrapment of air bubbles in the feed powder particles is significantly reduced in wire feeding system. Also, dilution control by increasing material deposition rate can be easily achieved in wire feeding system with negligible material wastage.

In this work, single beads and multiple (i.e. overlapped) beads of Inconel 625 wire with minimal dilution, strong bonding with the substrate, free of cracks, pores (within the clad layers) and inter-run pores are deposited under optimised cladding conditions. The microstructure of a typical Inconel 625 wire laser bead is investigated and then related to its micro-hardness and corrosion performance in saline environment. Its corrosion performance is then compared to that of the 304 stainless steel (substrate), wrought Inconel 625 and another deposited Inconel 625 wire bead of higher dilution ratio.

2. Experimental

2.1. Materials

Austenitic stainless steel AISI 304 supplied by Smith Metals Nottingham was used as the substrate material. Plates (100 mm × 180 mm × 6 mm) were prepared and then grit blasted and degreased with acetone before the cladding process so as to improve the substrate surface laser absorptivity and remove contaminants respectively. The chemical composition of the stainless steel, as received, is given in Table 1. The chemical composition of Inconel 625 wire as received from VBC group, Loughborough, UK is also shown in Table 1. The diameter of the wire is 1.2 mm.

2.2. Laser processing

Fig. 1 shows the experimental arrangement for the laser deposition system used in this study. Deposition was performed using a 2 kW Ytterbium doped fibre laser (IPG Photonics) operating at 1070 nm wavelength. The beam was focused to a circular spot of approximately 3.1 mm at 20 mm beyond the focal plane giving a 212 mm working distance with a Gaussian energy distribution. Inconel 625 wire was "front fed" at an angle of $42° ± 1$ to the horizontal so as to aim the wire tip at the centre of the meltpool. A WF200DC wire feeder (Redman Controls and Electronic Ltd.) was used. Prior the start of the depositions, a working distance of 10 mm was kept between the substrate and the feed wire tip.

Processing conditions for cladding Inconel 625 wire with a fibre laser at which a combination of favourable single track properties including low wetting angle (<80°) (see Fig. 2), minimal dilution ratio (5–13%) and high surface quality can be obtained has been determined by Abioye et al. (2013) in their previous work. The processing parameters are given in Table 2. Single and multiple beads (single layer) of Inconel 625 wire were deposited according to Table 2. A minimum of 1 min cooling time was allowed between two successive runs during the deposition of both single and multiple beads. Multiple beads were deposited using a 60% overlap ratio. All depositions were performed inside a transparent enclosure (bag) which was evacuated and back-filled with argon gas supplied at 0.42 l/s.
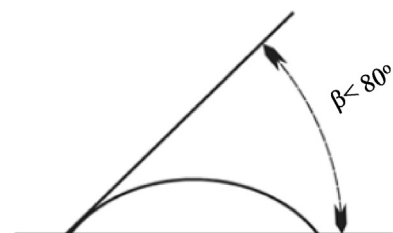

Fig. 2. A schematic diagram showing a good wetting angle ($\beta < 80°$) in a single bead.

Table 1
Chemical compositions of Inconel 625 wire and 304 stainless steel in wt%.

Element	Ni	Cr	Mn	Si	Al	Ti	Fe	C	Mo	Nb	P	S
Inconel 625	Bal	22.46	–	–	0.26	0.26	0.14	0.02	8.84	3.46	–	–
304 stainless steel	7.86	18.58	1.78	0.42	–	–	Bal	0.08	–	–	0.10	0.03

2.3. Microstructural analysis

Each deposited clad bead was longitudinally and transversely cross-sectioned and electrolytically etched using a 70% orthophosphoric acid in water (typically 6 V for 3 s). The clad grain structures were first studied using a Nikon optical microscope. Further microstructural examination was performed on polished clad samples using scanning electron microscopy (SEM; FEI XL30) with both secondary electron (SE) and backscattered electron (BSE) signals. SEM was also used in combination with energy dispersive X-ray analysis (EDX) so as to determine the elemental composition of microstructural features (or phases) observed in the clad samples. X-ray diffraction (XRD) was utilised in order to identify the phases present in the clad samples. A Bruker D500 with Cu-Kα radiation of wavelength 0.1 nm was used. For all the analysis, XRD scans were performed at 40 kV with a step size of 0.01° and a dwell time of 2 s per step in the 2θ range of 25–110°. The degree of Fe dilution ratio in the clad beads was determined using Eq. (1) (Toyserkani et al., 2005). ρ_c and ρ_s in Eq. (1) are the densities of the additive (8.44×10^{-3} g mm^{-3}) and substrate (8.0×10^{-3} g mm^{-3}) materials respectively. X_{c+s} and X_s are the mean weight percent of Fe in the clad region and substrate respectively. X_c is the weight percent of Fe in the additive material.

$$\eta = \frac{\rho_c (X_{c+s} - X_c)}{\rho_s (X_s - X_{c+s}) + \rho_c (X_{c+s} - X_c)} \tag{1}$$

The Fe content of the deposited multiple beads was determined using EDX technique. Area scans ($200 \times 200\ \mu m^2$) was conducted randomly at 20 locations within their cross sections.

2.4. Microhardness testing

A Vickers hardness tester with a load of 0.3 kg was used to measure the micro-hardness along the depth in the transverse cross-sections of single clad bead. The measurements were made along the middle of the clad cross-sections with a spacing of 0.15 mm between successive points.

2.5. Corrosion testing

The corrosion behaviour of Inconel 625 clad beads and stainless steel substrate were investigated using potentiodynamic polarisation testing. The tests were carried out according to the guidelines stated in ASTM standards G5-94 and G61-86 respectively (ASM Handbook, 2003). A 100 mm^2 surface area of the samples was exposed to the saline media (3.5 wt% NaCl) at room temperature using a three electrode cell. The electrolyte was de-aerated

by nitrogen gas purging for a minimum of 30 min prior to sample immersion in order to ensure that the experiment was carried out in an oxygen free environment. This continued for the duration of the experiment. Each sample (i.e. working electrode) was allowed to settle for 60 min before polarising the potential against Ag/AgCl electrode (the reference electrode). A platinum plate was used as the counter electrode. With the use of Potentiostat (ACM instruments, Cumbria, UK), potentiodynamic polarisation scans were performed for each of the samples with a sweep rate of 20 mV min^{-1} from the 1 h open circuit potential. Three samples from the optimum clad layer and another three from the substrate were prepared and tested. The potential was scanned over the range of −200 to 1500 mV. The corresponding current flow between the working and counter electrodes was recorded for each scan. The corroded surface of the sample, after each scan, was then examined by optical and scanning electron microscopy. Image processing software was used to measure the corroded area
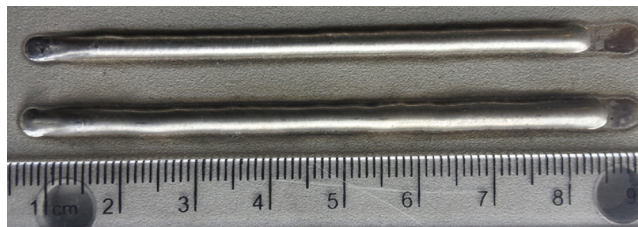
3. Results and discussion

3.1. Geometrical characterisation

All the single clad beads were continuous and free of surface defects. For example, two Inconel 625 single clad beads which are representatives of others are shown in Fig. 3. The geometry of the single clad beads has been investigated in prior work (Abioye et al., 2013). A typical single clad bead formed at 1.8 kW laser power, 1.7 mm s^{-1} traverse speed and 10 mm s^{-1} wire feed rate was selected for microstructural analysis. This specimen showed a combination of good clad qualities including minimal dilution (11.9%), high aspect ratio (2.6) and low wetting angle (75°). Minimal dilution is good for corrosion resistance of the coating while a high aspect ratio (>2.5) and low wetting angle (<90°) are required for multiple bead cladding which is free of inter-run porosity.

3.2. Microstructure

In all cases, the microstructure of the continuous single clad bead appears to comprise mainly columnar dendrites. However, changes in the grain structure and dendrite spacings were observed as the processing parameters varied. The optical micrograph of the longitudinal section of the typical clad bead is presented in Fig. 4. From the clad-substrate interface, there was an evolution of columnar dendrites growing perpendicularly to the substrate. Near the top region, there was a transition to near horizontal columnar dendrites (parallel to the substrate).

Table 2
Processing conditions utilised for the depositions.

S/N	Laser power (kW)	Traverse speed (mm s^{-1})	Wire feed rate (mm s^{-1})
1	1.8	1.7	10.0
2	1.8	3.3	13.3
3	1.8	5.0	13.3
4	1.6	3.3	10.0
5	1.6	5.0	13.3
6	1.4	5.0	10.0
7	1.2	3.3	6.7

Fig. 3. Macrophotograph of continuous Inconel 625 wire single clad beads free of surface cracks.
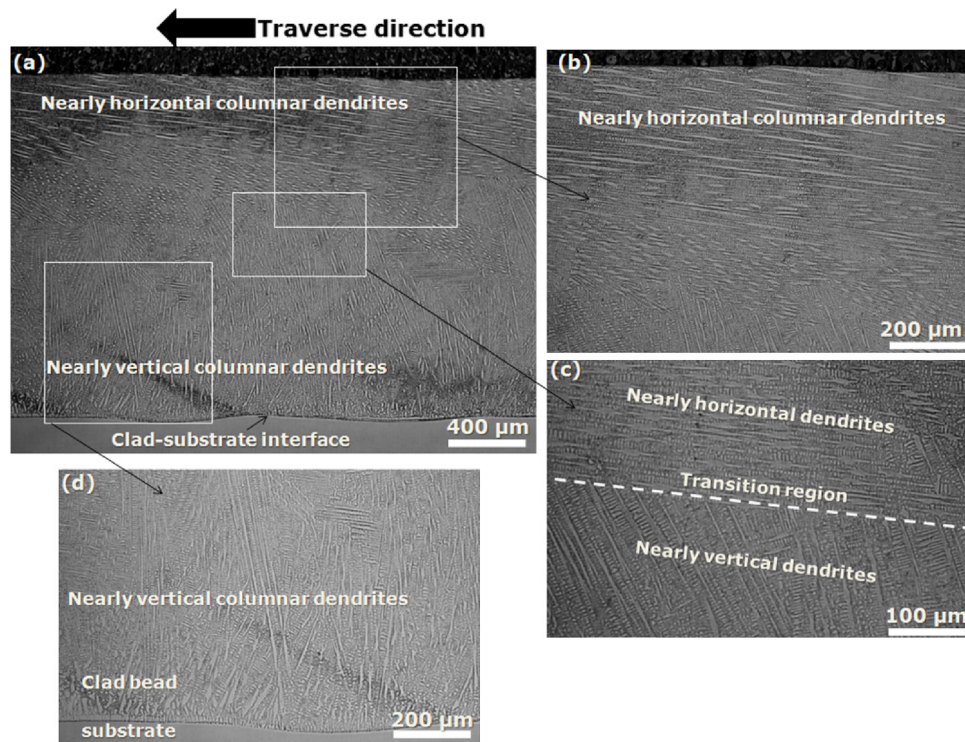
Fig. 4. Optical micrographs showing different regions of the (a) longitudinal section of a typical Inconel 625 wire clad bead. (b) near surface region, (c) transition from vertical columnar dendrites to horizontal columnar dendrites and (d) bottom region.

At the clad-substrate interface, heat transfer is mainly by conduction from the meltpool to the substrate. The reason for the vertical growth of the dendrite from the substrate is due to the fact that the substrate acts as the heat sink in this region as dendrites in fcc nickel alloys grow fastest along the ⟨1 0 0⟩ directions most closely aligned to the maximum temperature gradient. The growth of horizontal columnar dendrites near the surface region is attributed to the change in principal heat flux direction. Since the clad core is very hot, the heat in the top region was largely extracted to the solidified clad at the back of the meltpool, as shown in Fig. 5. This probably led to directional growth of the dendrites from the back of the meltpool (growing against heat flux). Similar findings have been reported by Dinda et al. (2009) during the investigation of the microstructure of Inconel 625 powder laser clad. It was found that the microstructure of the Inconel 625 powder laser fabricated walls consist entirely of columnar dendrites which grew epitaxially from the substrate (Inconel 625 plate). Also, an orientation change in the dendrites growth was observed at the upper part of the top layer.

3.3. XRD analysis

The XRD spectrum of the typical single clad layer is presented in Fig. 6. The major peaks in the spectrum were found at $2\theta = 43.5°$, $50.7°$, $74.6°$, $90.5°$ and $95.8°$. However, the peak positions for pure Ni from the ICDD-database were found at $2\theta = 44.5°$, $51.9°$, $76.4°$, $92.9°$ and $98.5°$.

Pure FCC Ni phase peaks occur at slightly higher values of 2θ when compared with the positions where major peaks were observed in the XRD spectra of the laser clad of Inconel 625 wire.
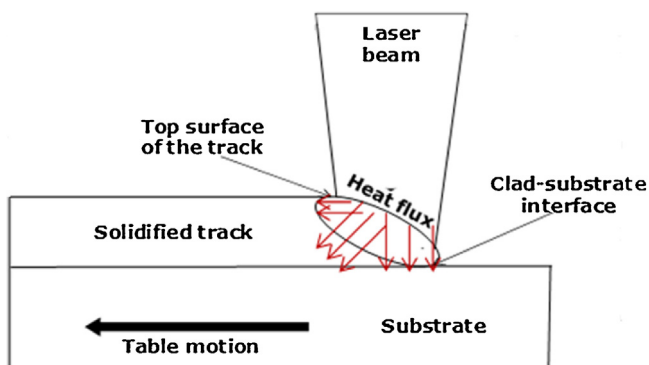
Fig. 5. A diagram illustrating the heat flow direction in the meltpool.
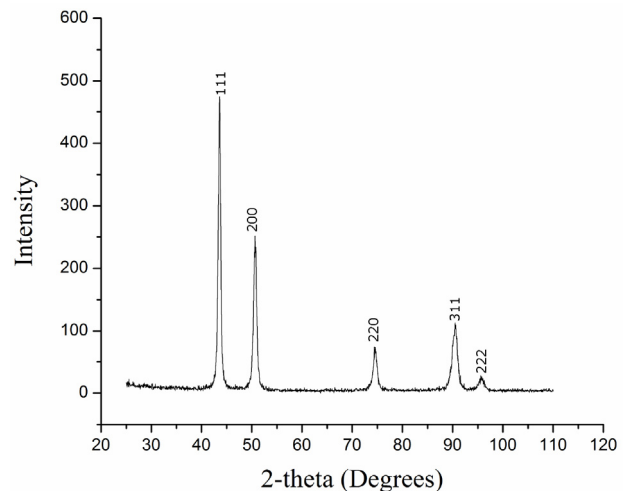
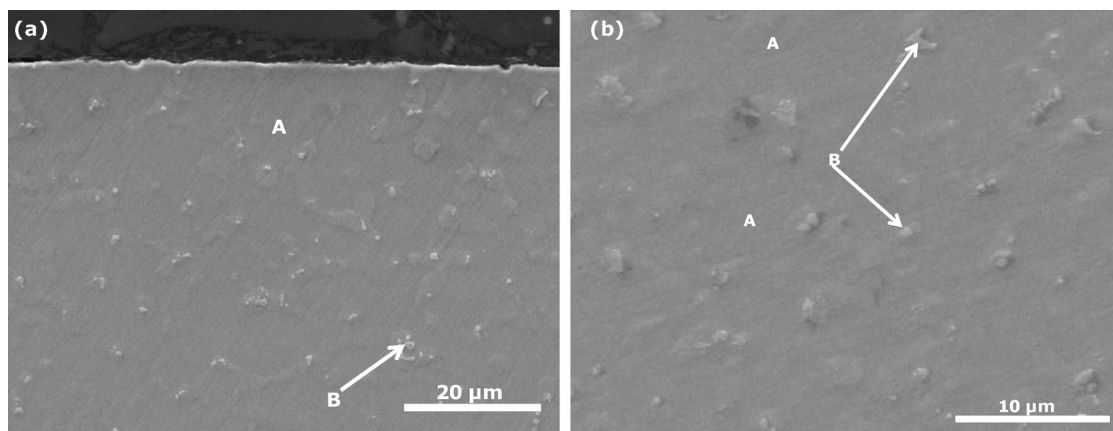**Fig. 6.** XRD spectrum of the typical Inconel 625 wire laser clad bead.

Fig. 7. Secondary electron images showing the phases in the microstructure of the typical Inconel 625 wire laser clad bead.

The difference in the lattice parameter is due to alloying elements in the solid solution of Inconel 625. This affected the inter-planar spacing of the γ-Ni present in the coating. No phases other than an FCC γ-Ni phase with lattice parameter close to pure Ni could be detected. However, the limit of detection for secondary phases by XRD is approximately 1–2%.

3.4. Elemental composition of the identified phases

SEM/EDX analysis of the single clad beads revealed continuous dark dendritic matrix and light contrast precipitates in the interdendritic regions, for example, as shown in Fig. 7. EDX spot analysis was performed on the dark continuous matrix marked 'A' and the light contrast precipitate marked 'B'. The results, for the typical single clad bead, are summarised in Table 3 which is the average of five measurements. It is evident that the matrix composition is significantly richer in Fe (9.2 wt%) when compared with the wire feedstock which has a Fe composition of 0.14 wt%. This can be attributed to dilution of Fe from the stainless steel substrate. The matrix marked 'A' is considered to be the γ-Ni phase because it is richer in Ni, Cr and Fe when compared to the precipitate marked 'B'. Conversely, the precipitates are richer in Mo and Nb compared to the matrix. In the past, Rombouts et al. (2012) have identified Mo- and Nb-rich precipitates in the microstructure of laser clad Inconel coatings.

Also, a study on the solidification of Inconel 625 and Inconel 718 has been done by DuPont (1996). Depending on the compositions of C, Si and Fe in the Ni-based superalloys, the Mo- and Nb-rich precipitates (most notably enriched in Nb) were identified as either Laves phase and/or NbC. In this case, the light contrast precipitates are considered to be Mo- and Nb-rich precipitates.

3.5. Micro-hardness

Vickers micro-hardness measurements were obtained, starting from the substrate, along the centreline of the transverse section of the clad bead samples. Fig. 8 presents the micro-hardness profiles of the typical single clad bead. It is apparent that the Inconel 625 clad exhibits higher hardness than the substrate.

The substrate hardness was not significantly altered as its value before and after the deposition were 201 ± 2.4 HV$_{0.3}$ and 205 ± 1.5 HV$_{0.3}$ respectively. The average micro-hardness of the typical single clad bead was 232 ± 4.5 HV$_{0.3}$.

3.6. Overlapped clad layers

Multiple clad beads, using a 60% overlapping ratio, were deposited at the optimised processing conditions presented in Table 2. Their top surfaces are rather flat, free of cracks and of good surface finish, for example, as shown in Fig. 9.

The cross-sections of the multiple clad beads deposited at the optimised parameters revealed good bonding with the substrate, no cracks and no pores including inter-run pores, for example, as shown in Fig. 10. In all cases, a significant reduction in the Fe content was observed when compared to their corresponding single clad bead, for example, as presented in Table 4. The reduction in the Fe dilution is calculated from Eq. (1). It is due in part to additional heating of the adjacent clad during the multiple bead cladding.

3.7. Corrosion performance

The corrosion performance of the typical multiple bead layer (dilution ratio = 4.5%) deposited at 1.8 kW laser power, 1.7 mm min^{-1} traverse speed and 10 mm min^{-1} wire feed rate and the substrate was evaluated in de-aerated 3.5 wt% NaCl solution at
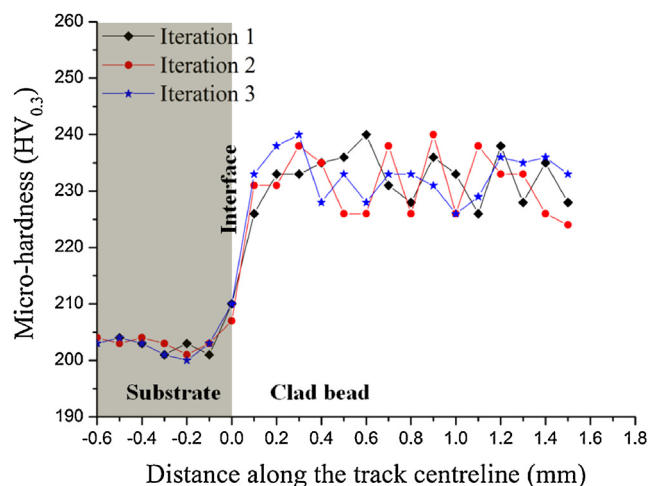

Fig. 8. Micro-hardness profile of the typical single laser clad bead of Inconel 625 wire.

Table 3
Elemental composition (wt%) of phases present in the typical single clad layer of Inconel 625 wire laser cladding.

Symbol	Phase	Cr	Fe	Ni	Nb	Mo
A	FCC Ni matrix	23.2 ± 0.2	9.2 ± 0.4	56.4 ± 0.5	2.3 ± 0.4	8.6 ± 0.3
B	Precipitate	19.2 ± 0.4	6.8 ± 0.3	46.7 ± 0.5	12.6 ± 1.3	14.2 ± 0.8

Table 4
Fe content in the laser clad single bead and the corresponding multiple beads.

Processing parameters			Single track		Overlapped tracks		Reduction in Fe dilution (%)
Laser power (kW)	Traverse speed (mm s^{-1})	Wire feed rate (mm s^{-1})	Fe content (wt%)	Dilution (%)	Fe content (wt%)	Dilution (%)	
1.8	1.7	10	9.2 ± 0.4	11.9	3.3 ± 1.5	4.5	62.2
1.8	5.0	13.3	21.8 ± 0.6	24.3	9.3 ± 1.9	12	52.9

Table 5
Corrosion test data for Inconel 625 wire laser coatings, wrought Inconel 625 alloy and as-received 304 stainless steel in de-aerated 3.5 wt% NaCl solution at room temperature.
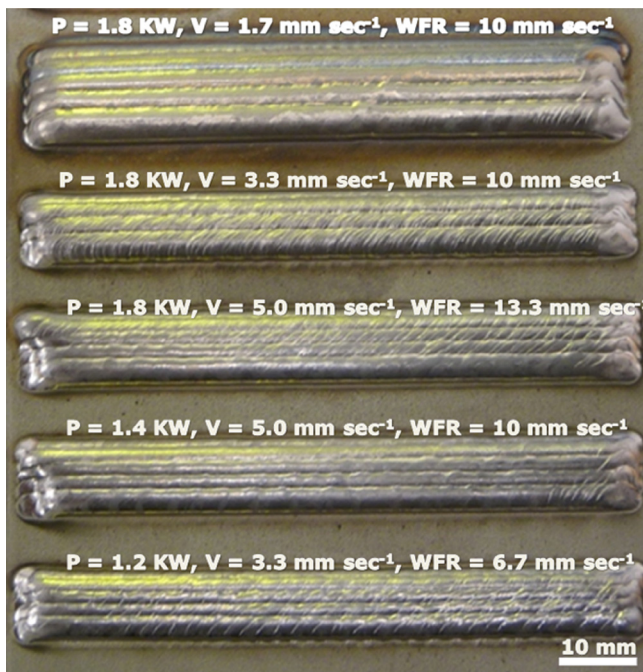
Material/coating	Fe Dilution (%)	Reference electrode	Corrosion performance		
			E_{corr} (mV)	I_p (mA cm^{-2})	E_b (mV)
Inconel 625 wire (Typical) clad	4.5	Ag/AgCl	−222 ± 8	3.0×10^{-4}	585 ± 5
Inconel 625 wire clad	12	Ag/AgCl	−273 ± 18	2.2×10^{-3}	472 ± 8
304 Stainless steel	–	Ag/AgCl	−265 ± 16	1.9×10^{-3}	340 ± 10
Wrought Inconel 625	–	Ag/AgCl	−264	4.7×10^{-4}	600

room temperature. In order to determine the effect of Fe dilution on the laser deposited Inconel 625 wire coatings, another multiple bead layer of Inconel 625 wire of higher dilution ratio (12%), as presented in Table 4, was investigated for corrosion performance under similar condition. Table 5 summarises the corrosion parameters (average of three scan measurements for each coating/material)
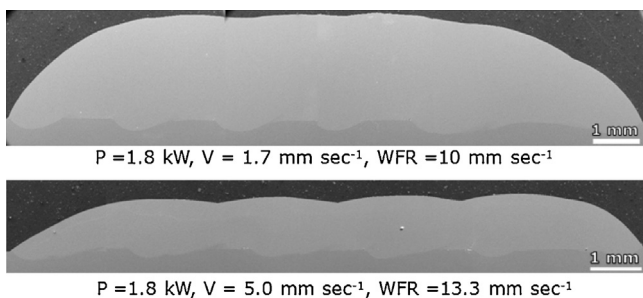

Fig. 9. Laser clad multiple beads of Inconel 625 wire showing flat surfaces and no surface cracking.

Fig. 10. SEM/SE image of the transverse cross-sectioned multiple beads of Inconel 625 wire showing good clad-substrate bonding.

in terms of corrosion potential (E_{corr}), passive current density (I_p) and breakdown potential (E_b). The corrosion performance of the wrought alloy 625 in de-aerated 3.5 wt% NaCl solution at room temperature as found in the literature (Tuominen et al., 2003) is also included in Table 5. Fig. 11 shows the potential polarisation behaviour of the Inconel 625 wire laser coatings and the AISI 304 stainless steel.

From the results presented in Table 5, it is clear that the corrosion performance of the typical multiple layer with 4.5% dilution ratio is very close to that of wrought Inconel 625. Compared with the substrate, the typical Inconel 625 wire multiple bead layer (4.5% dilution) exhibited improved corrosion resistance. The multiple bead layer passivated at lower current density (3×10^{-4} mA cm^{-2}) compared to the substrate which passivated at 1.9×10^{-3} mA cm^{-2}. Since the formation of passive film at low current density hinders severe loss of material at higher current density, lower passive current density therefore indicates improved corrosion resistance. Also, the ability of a material to resist a formation of localised attack on the passive film is a function of its breakdown potential.

The typical multiple bead layer ratio has wider passive region with a breakdown potential of 585 ± 5 mV (wrt Ag/AgCl electrode). The breakdown potential for the AISI 304 stainless steel (substrate) is 340 ± 10 mV (wrt Ag/AgCl electrode) and a rapid increase in current density with a little or no change in potential was observed after a narrow passive density. This potentially suggests an occurrence of pitting or crevice corrosion on the surface of the substrate.
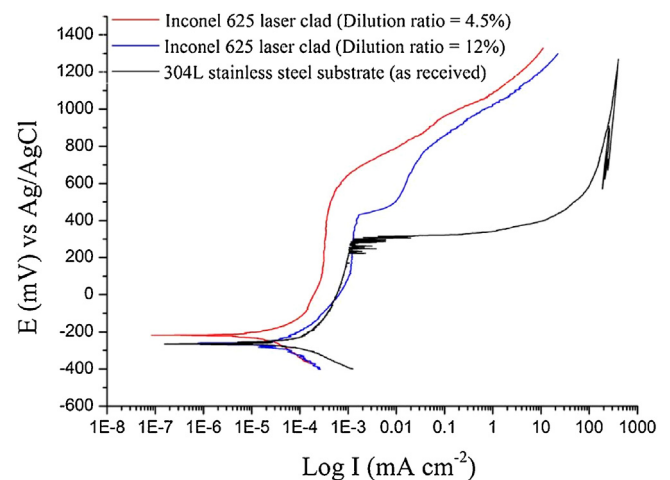
Fig. 11. Polarisation curves of Inconel 625 laser clad layers and 304L stainless steel (as received) substrate in de-aerated 3.5 wt% NaCl solution at room temperature.
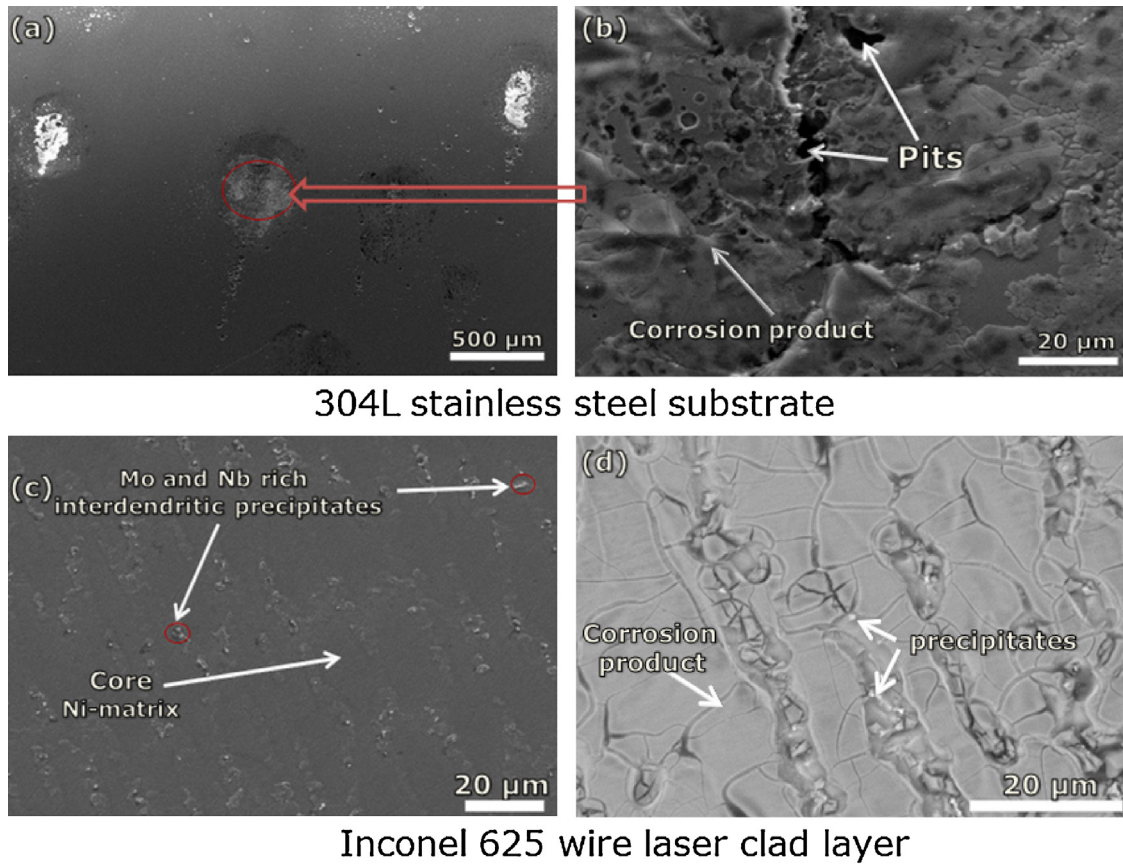
Fig. 12. SEM/BSE images of (a–b) corroded surface of 304L stainless steel substrate, Inconel 625 wire laser clad layer (c) before and (d) after the corrosion test in de-aerated 3.5 wt% NaCl solution.

Also, the positive hysteresis found in the polarisation curve (of the substrate) and corrosion pits observed in the SEM/BSE image showing the corroded surface, as shown in Fig. 12a–b, confirmed the occurrence of localised (pitting) corrosion in the substrate. The higher breakdown potential demonstrated by the typical multiple clad bead implies that damage nuclei could not be easily initiated on the passive layer as expected. Even, in the transpassive region (of the clad layer), the gradient of the current density against potential is lower indicating that permanent damage could not form on the passive layer. Therefore, the corrosion damage on the typical multiple bead layer is uniform. Comparing the values of their corrosion potential, the laser clad layer appears to be nobler.
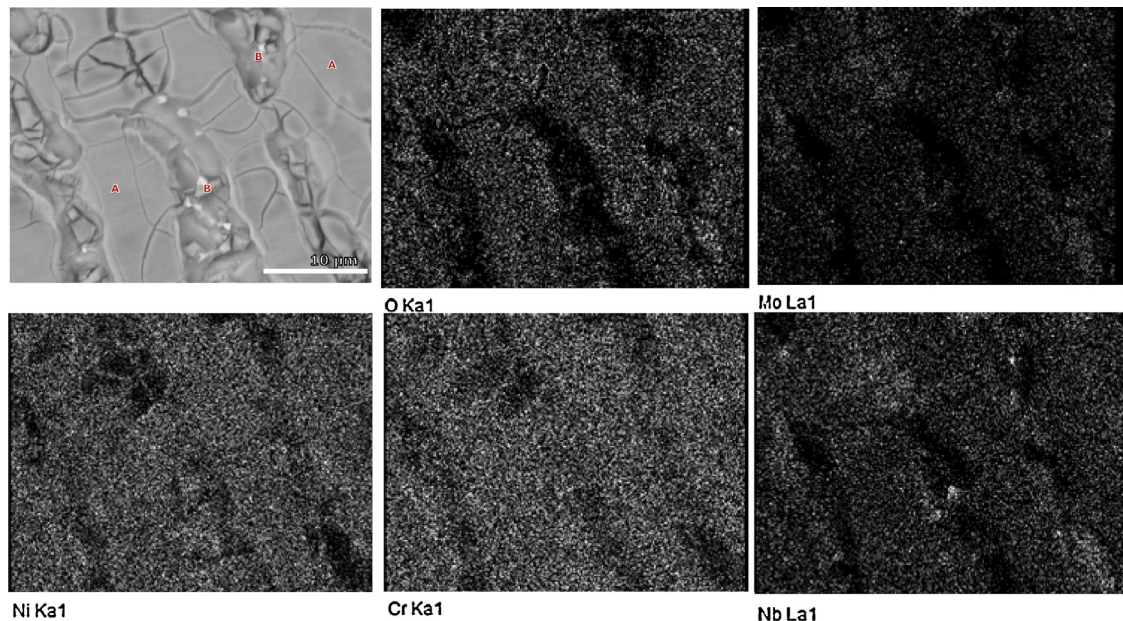
Fig. 13. X-ray mapping of the top surface of the typical Inconel 625 wire laser clad layer after potentiodynamic polarisation scan in de-aerated 3.5% NaCl solution.
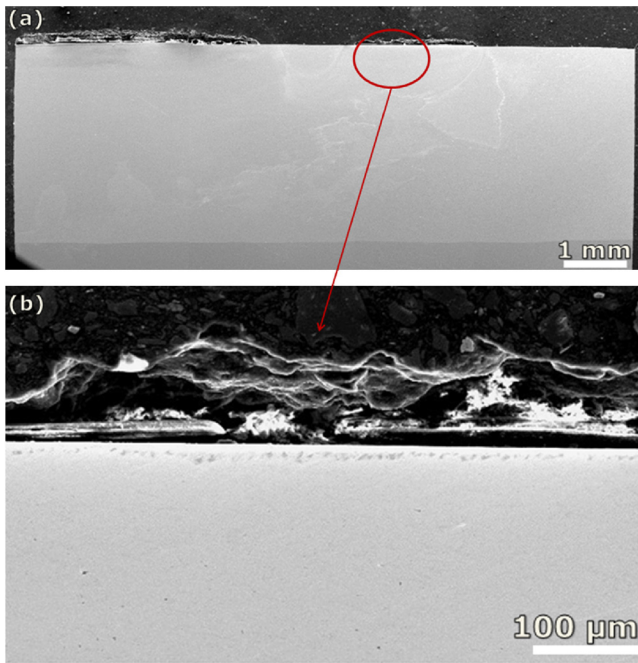
Fig. 14. Cross-sectional view of the typical Inconel 625 wire laser clad layer after polarisation in de-aerated 3.5% NaCl at (a) low and (b) high magnifications.

The effect of Fe dilution on the corrosion performance of the Inconel 625 wire clad beads was revealed by comparing the potentiodynamic polarisation scan curve of the typical multiple bead layer with another laser clad layer of Inconel 625 wire with higher dilution ratio (12%). The multiple bead layer with 12% dilution ratio demonstrated lower breakdown potential, lower corrosion potential and higher passive current density which all indicates lower corrosion resistance. The explanation for this is that corrosion performance of Inconel 625 wire laser coatings deteriorates with an increase in Fe dilution ratio.

Fig. 12c and d shows the SEM/BSE images of the top surface of the typical multiple bead layer before and after the corrosion test, respectively. It can be inferred that the surface corroded uniformly since there is no evidence of pits throughout the corroded surface. The matrix region was believed to be selectively attacked because the dark continuous matrix was covered by the grey-like corrosion product. The precipitates appear to be unaffected as there was no significant change to their abundance at the surface or their morphology. The corrosion mechanism is believed to be in form of galvanic coupling in which the dendritic matrix acts as the sacrificial anode because it was preferentially attacked. In order to confirm this, SEM/EDX mapping of the corroded surface of the clad layer was carried out, as shown in Fig. 13.

The results of the detailed composition (EDX) analysis undertaken at the two regions marked 'A' and 'B' in Fig. 13 are presented in Table 6. It was found that the grey region marked 'A' covering the core dendritic matrix is rich in Mo (17.5 wt%) and O (19.5 wt%). The significant presence of O indicates that the core dendrites suffered from oxidation leading to formation of probably oxides or compounds of molybdenum. The light contrast (precipitates) marked 'B' at the boundaries in-between the dendritic core contains negligible amount of O (2.6 wt%) but still contain a considerable proportion

Table 6
Summary of the composition analysis (wt%) of the two different regions identified in SEM image in Fig. 13.

Symbol	O	Cr	Fe	Ni	Nb	Mo
A	19.5	15.7	1.2	37.2	9	17.5
B	2.6	21.6	0.9	58.8	5.3	10.8

of Mo and Nb. The negligible O content and imperceptible change in contrast show that the phase marked 'B' did not suffer corrosion attack.

The typical multiple bead was sectioned transversely, after corrosion test, so as to show the thickness of the corrosion product on the top surface. As shown in Fig. 14, the maximum thickness of the corrosion product is a lower than 0.1 mm, indicating slow corrosion rate. Also, there was no ingress of the electrolyte or the existence of corrosion products within the clad bead layer. This shows that the substrate is fully protected by the Inconel 625 wire laser clad.

4. Conclusions

- This study has found that pore- and crack-free, minimally diluted and well bonded Inconel 625 multiple beads deposited by laser cladding using wire as the feedstock material is possible.
- Compared to single bead, the corresponding multiple bead layer shows reduced Fe dilution. A minimum Fe dilution of 4.5% was found for single and multiple laser clad beads of Inconel 625 wire in this study.
- The corrosion performance of the Inconel 625 wire laser coating, at 4.5% Fe dilution, is very close to that of the wrought Inconel 625 alloy. However, a lower corrosion performance was obtained when the Fe dilution increased to 12%.
- Unlike 304L stainless steel substrate which demonstrated pitting corrosion, the Inconel 625 wire laser coatings corrode uniformly in de-aerated 3.5 wt% NaCl solution.
- Components made of stainless steels can be well protected by the Inconel 625 wire laser coatings since the thickness of the corrosion product was below 0.1 mm at the top surface of the multiple clad beads which is about 4 mm thick.

References

Abioye, T.E., Folkes, J., Clare, A.T., 2013. A parametric study of Inconel 625 wire laser deposition. J. Mater. Process. Technol. 213 (12), 2145–2151.

Ahmed, N., 2008. Characterisation of Different Forms of Inconel 625 for Determining the Effects of Microstructural Modifications on Electrochemical Behaviour. Department of Mechanical, Materials and Manufacturing Engineering, University of Nottingham, Nottingham (Ph.D. thesis).

Al-fadhli, H.Y., Stokes, J., Hashmi, M.S.J., Yilbas, B.S., 2006. The erosion-corrosion behaviour of high velocity oxy-fuel (HVOF) thermally sprayed Inconel-625 coatings on different metallic surfaces. Surf. Coat. Technol. 200 (20–21), 5782–5788.

Dinda, G.P., Dasgupta, A.K., Mazumder, J., 2009. Laser aided direct metal deposition of Inconel 625 superalloy: microstructural evolution and thermal stability. Mater. Sci. Eng.: A 509 (1–2), 98–104.

Donachie, M., Donachie, J., 2002. Superalloys. A Technical Guide. ASM International, USA.

DuPont, J.N., 1996. Solidification of an alloy 625 weld overlay. Metall. Mater. Trans. A 27A, 3612–3620.

ASM Handbook, 2003. Corrosion: Fundamentals, Testing and Protection, vol. 13A. ASM International.

Huang, Y., 2011. Characterization of dilution action in laser-induction hybrid cladding. Opt. Laser Technol. 43 (5), 965–973.

Kim, H.I., Park, H.S., Koo, J.M., Yang, S.H., kim, M.Y., Seok, C.S., 2007. Welding characteristics evaluation of GMAW and laser cladding for the gas turbine 1st blade. Key Eng. Mater. 353–358, 519–522, 2007.

Nurminen, J., 2008. Hot-Wire Laser Cladding: Process, Materials and Their Properties. Tampere University of Technology (Ph.D.).

Paul, C.P., Ganesh, P., Mishra, S.K., Bhargava, P., Negi, J., Nath, A.K., 2007. Investigating laser rapid manufacturing for Inconel-625 components. Opt. Laser Technol. 39 (4), 800–805.

Rombouts, M., Maes, G., Mertens, M., Hendrix, W., 2012. Laser metal deposition of Inconel 625: microstructure and mechanical properties. J. Laser Appl. 24 (5), 2012.

Toyserkani, E., Khajepour, A., Corbin, S., 2005. Laser Cladding. CRC Press.

Tuominen, J., Vuoristo, P., Mantyla, T., Latokartano, J., Vihinen, J., Andersson, P.H., 2003. Microstructure and corrosion behaviour of high power diode laser deposited Inconel 625 coatings. J. Laser Appl. 15 (1).

Tuominen J., Näkki J., Junkala J., Miettinen J., Peltola T., Vuoristo P., 2012. Corrosion resistant laser coatings for hydraulic piston rods. Proceedings of the 31st International Congress on Applications of Lasers & Electro-Optics, Anaheim, CA, USA.

Zareie Rajani, H.R., Akbari Mousavi, S.A.A., Madani Sani, F., 2013. Comparison of corrosion behavior between fusion cladded and explosive cladded Inconel 625/plain carbon steel bimetal plates. Mater. Des. 43 (0), 467–474.

Zhou, S., Huang, Y., Zeng, X., Hu, Q., 2008a. Microstructure characteristics of Ni-based WC composite coatings by laser induction hybrid rapid cladding. Mater. Sci. Eng.: A 480 (1–2), 564–572.

Zhou, S., Zeng, X., Hu, Q., Huang, Y., 2008b. Analysis of crack behavior for Ni-based WC composite coatings by laser cladding and crack-free realization. Appl. Surf. Sci. 255 (5, Part 1), 1646–1653.